Implicit-Explicit Runge-Kutta Methods for Time-Dependent Partial Differential Equations

Uri M. Ascher* Steven J. Ruuth† Raymond J. Spiteri‡

March 13, 1997

Abstract

Implicit-explicit (IMEX) linear multistep time-discretization schemes for partial differential equations have proved useful in many applications. However, they tend to have undesirable time-step restrictions when applied to convection-diffusion problems, unless diffusion strongly dominates and an appropriate BDF-based scheme is selected [2].

In this paper, we develop Runge-Kutta-based IMEX schemes that have better stability regions than the best known IMEX multistep schemes over a wide parameter range.

1 Introduction

When a time-dependent partial differential equation (PDE) involves terms of different types, it is a natural idea to employ different discretizations for them. Implicit-explicit (IMEX) time-discretization schemes are an example of such a strategy. Linear multistep IMEX schemes have been used by many researchers, especially in conjunction with spectral methods [10, 3]. Some schemes of this type were proposed and analyzed as far back as the late 1970's [15, 5]. Instances of these methods have been successfully applied to the incompressible Navier-Stokes equations [9] and in environmental modeling studies [16]. A systematic, comparative study for PDEs of convection-diffusion

*Institute of Applied Mathematics and Department of Computer Science, University of British Columbia, Vancouver, BC, V6T 1Z4, Canada. (ascher@cs.ubc.ca). The work of this author was partially supported under NSERC Canada Grant OGP0004306.

†Department of Mathematics, University of California, Los Angeles. (ruuth@math.ucla.edu). The work of this author was partially supported by an NSERC Postdoctoral Scholarship and NSF DMS94-04942.

‡Institute of Applied Mathematics and Department of Mathematics, University of British Columbia, Vancouver, BC, V6T 1Z2, Canada.(spiteri@math.ubc.ca). The work of this author was partially supported under NSERC Canada Grant OGP0004306.

type was carried out in [2], and a corresponding study for reaction-diffusion problems arising in morphology is reported in [11].

In this work, we consider problems of convection-diffusion type (or hyperbolic-parabolic equations), e.g.

$$u_t = uu_x + \nu \Delta u, \qquad \nu > 0. \tag{1.1}$$

Discretization of the spatial derivatives (e.g. by finite-difference, finite-element, finite-volume, or spectral methods) yields a very large ODE system in time,

$$\dot{u} = f(u) + g(u), \tag{1.2}$$

where f corresponds to the convection (hyperbolic) term, uu_x, and g corresponds to the diffusion (parabolic) term, $\nu\Delta u$. An IMEX scheme consists of applying an implicit discretization for g and an explicit one for f. This is natural because the system (1.2) with $f \equiv 0$ is generally stiff and linear, whereas with $g \equiv 0$ the system is not too stiff and it is often nonlinear. Moreover, if one insists on using an implicit discretization for the latter case, the construction of iterative solvers is made challenging by the properties of the matrix to be inverted.

In [2] we have analyzed and experimented with linear multistep schemes for (1.2). For diffusion-dominated problems, schemes utilizing Backward Differentiation Formulae (BDF) for g have optimal damping properties. The corresponding IMEX scheme is a semi-explicit BDF (SBDF) [15, 5, 9]. However, when diffusion is not dominant, the choice of method is less obvious. Ideally, one would like a dissipative scheme for the hyperbolic term, so that the resulting IMEX scheme would have good stability and smoothing properties, independent of $g(u)$. Yet, it is well known that this necessitates looking for schemes of order (or more accurately, backward steps) at least 3 (cf. [2]). The main difficulty plaguing multistep IMEX schemes is the possibility that relatively small time steps become necessary due to stability restrictions (e.g. [14]). Such restrictions become worse when working with higher-order multistep schemes, as demonstrated in [2]. On the other hand, the stability region of explicit Runge-Kutta schemes actually increases slightly when three- and four-stage schemes are contemplated. Thus, we are led to investigate the development and performance of IMEX Runge-Kutta schemes.

When the system (1.2) arises from a PDE in more than one spatial variable, the simplicity and efficiency of solving the algebraic equations corresponding to the implicit part of the discretization at each time step is of paramount importance. In [2], we show that, under appropriate circumstances and for certain IMEX schemes, not much more than one multigrid W-cycle per time-step is needed. Here, we aim at such a performance per Runge-Kutta stage. Hence, we concentrate on diagonally-implicit Runge-Kutta (DIRK) schemes for $g(u)$, paying particular attention to their attenuation properties. We construct a number of IMEX schemes of this sort, and investigate their properties. Since the effective order of DIRK schemes drops to 1 for very stiff ODEs [8], we do not expect the Runge-Kutta schemes to be competitive with SBDF in the limit where $g(u)$ is heavily dominant and very stiff. However, our Runge-Kutta schemes are shown to have excellent properties for other parameter ranges.

It is well known that, despite its recent rise in popularity, the use of Runge-Kutta schemes for the integration of time-dependent PDEs is not without drawbacks. One problem is a loss of accuracy order when time-dependent inflow boundary conditions are prescribed [4]. A remedy is proposed in [1]. Note also that, in the (usual) case where the accuracy of the solution at the end of the step is higher than at internal stages, the accuracy to which these internal stages must be calculated (say by an iterative method, as in §5) cannot be lowered.

The system (1.2) can be cast as a partitioned system,

$$\dot{v} = \hat{f}(v, w) \tag{1.3a}$$

$$\dot{w} = \hat{g}(v, w) \tag{1.3b}$$

with $u = v + w$, $\hat{f} = f(v + w)$ and $\hat{g} = g(v + w)$. The IMEX Runge-Kutta schemes devised below are then partitioned Runge-Kutta schemes. Their orders are discussed in [7], §II.15. They can also be seen as a particular class of splitting methods. We note that for (1.2), v and w need not be known individually (indeed we may not have initial conditions for them). All we need to have is their smooth, local existence.

In §2, we develop a number of IMEX Runge-Kutta schemes of up to four stages, which are up to third-order accurate. The schemes divide naturally into two classes – those whose last internal stage is identified with the solution at the next time instance (i.e. at the end of the time-step), and those where an additional quadrature is used at the end of the step. The first class is particularly good for highly-stiff problems, but it is the second class which seems to yield some of the more promising variants for a wide range of parameters, particularly the scheme identified as (3,4,3) (3 internal stages for the implicit formula, 4 stages for the explicit and a combined accuracy of order 3).

In §3, we investigate the performance of the various schemes for a simple test equation, which arises from a von Neumann analysis of an advection-diffusion equation. Stability regions are plotted in Figures 3.1 and 3.2. Results of test runs for a linear advection-diffusion equation are reported in §4.1 and the Burgers equation is experimented with in §4.2. In §5, we investigate the performance of our various schemes in conjunction with employing a multigrid method for resolving the implicitness at each stage.

2 IMEX Runge-Kutta schemes

We now develop some IMEX Runge-Kutta schemes. For g, we consider an implicit s-stage DIRK scheme [8] with coefficients $A \in \mathcal{R}^{s \times s}$, $c, b \in \mathcal{R}^s$, in the usual Butcher notation. Let $\sigma = s+1$. For f, we consider an $(s+1)$-stage explicit scheme with the abscissae $\hat{c} = \begin{pmatrix} 0 \\ c \end{pmatrix}$ and coefficients $\hat{A} \in \mathcal{R}^{\sigma\times\sigma}, \hat{b} \in \mathcal{R}^{\sigma}$. To cast the DIRK scheme as an $(s+1)$-stage scheme as well, we can pad the s-stage scheme with zeroes, obtaining the tableau

$$\begin{array}{c|cccccc}
0 & 0 & 0 & 0 & \cdots & 0 \\
c_1 & 0 & a_{11} & 0 & \cdots & 0 \\
c_2 & 0 & a_{21} & a_{22} & \cdots & 0 \\
\vdots & \vdots & \vdots & \vdots & \ddots & \vdots \\
c_s & 0 & a_{s1} & a_{s2} & \cdots & a_{ss} \\
\hline
 & 0 & b_1 & b_2 & \cdots & b_s
\end{array}$$

Referring to the coefficients of this padded tableau as $\tilde{A} \in \mathcal{R}^{\sigma\times\sigma}, \tilde{b} \in \mathcal{R}^{\sigma}, \tilde{c} \in \mathcal{R}^{\sigma}$, we see that $\tilde{c} = \hat{c}$. This property simplifies significantly the form of the order conditions on the method's coefficients due to coupling between the individual schemes.

One step from t_{n-1} to $t_n = t_{n-1} + k$ of the IMEX scheme is given as follows: Set

$$\hat{K}_1 = f(u_{n-1}). \tag{2.1a}$$

For $i = 1, \ldots, s$ do:

- Solve for K_i.

$$K_i = g(u_i), \tag{2.1b}$$

  where

$$u_i = u_{n-1} + k\sum_{j=1}^{i} a_{i,j}K_j + k\sum_{j=1}^{i} \hat{a}_{i+1,j}\hat{K}_j. \tag{2.1c}$$

- Evaluate

$$\hat{K}_{i+1} = f(u_i). \tag{2.1d}$$

Finally, evaluate

$$u_n = u_{n-1} + k\sum_{j=1}^{s} b_jK_j + k\sum_{j=1}^{\sigma} \hat{b}_j\hat{K}_j. \tag{2.1e}$$

We consider two special cases, which lead to two sub-families of methods: those which satisfy (2.2) and those which satisfy (2.3),(2.4):

1. In the case that $\hat{b} = \tilde{b}$ (and in particular $\hat{b}_1 = 0$), we have in place of (2.1e)

$$u_n = u_{n-1} + k \sum_{j=1}^{s} b_j (K_j + \hat{K}_{j+1}). \tag{2.2}$$

2. In the case that $\hat{b}_{s+1} = 0$, $\hat{K}_{s+1}$ need not be evaluated. Furthermore, if

$$b_j = a_{s,j}, \quad \hat{b}_j = \hat{a}_{s+1,j}, \quad j = 1, \ldots, s \tag{2.3}$$

(implying that the implicit scheme is stiffly accurate and $c_s = 1$), then substituting (2.1e) into the expression for u_s, we see that

$$u_n = u_s. \tag{2.4}$$

This is useful for very stiff problems. We note also that the explicit scheme can now be generated from a general explicit s-stage scheme based on the abscissae $c_1, \ldots, c_{s-1}$,

$$\begin{array}{c|ccccc} 0 & 0 & 0 & 0 & \cdots & 0 \\ c_1 & \hat{a}_{21} & 0 & 0 & \cdots & 0 \\ c_2 & \hat{a}_{31} & \hat{a}_{32} & 0 & \cdots & 0 \\ \vdots & \vdots & \vdots & \vdots & \ddots & \vdots \\ c_{s-1} & \hat{a}_{s1} & \hat{a}_{s2} & \hat{a}_{s3} & \cdots & 0 \\ \hline & \hat{b}_1 & \hat{b}_2 & \hat{b}_3 & \cdots & \hat{b}_s \end{array}$$

In (2.1b), there are s nonlinear systems to solve involving g alone, and the operators to be inverted are

$$I - k a_{ii} g_u.$$

Assuming that the Jacobian g_u is evaluated only once (at t_{n-1}), this operator is the same for each i if a_{ii} is independent of i, i.e. for SDIRK schemes. However, if an iterative method like 1-cycle multigrid is used for the implicit scheme, then perhaps it is less critical for the overall efficiency to insist on SDIRK, and a more general DIRK scheme can be contemplated. See [8], §IV.6, for stiffly-accurate SDIRK schemes. In our search for particularly accurate and stable schemes, we have allowed the diagonal elements of A to differ from one another. Despite this, the schemes we recommend are all SDIRK, since there were sufficient excess degrees of freedom in the solution process to allow for this computationally-efficient choice.

Example 2.1 *Consider the case of (1.2) where* $u = \begin{pmatrix} q \\ p \end{pmatrix}$, $f = \begin{pmatrix} 0 \\ f_2 \end{pmatrix}$, $g = \begin{pmatrix} f_1 \\ 0 \end{pmatrix}$. *Thus, we apply the implicit scheme to advance q and the explicit one to advance p. Observe that if f_2 is influenced by a control function, for instance, then at each stage*

i, this influence is propagated to K_i from $\hat{K}_i$. This does not happen when using a "normal" explicit scheme (cf. [13]). Moreover, if f_1 is independent of q then

$$I - ka_{ii}g_u = \begin{pmatrix} I & -ka_{ii}(f_1)_p \\ 0 & I \end{pmatrix}$$

and the scheme becomes explicit!

In particular, for Hamiltonian systems we can set $u = (q,p)^T$, $f = (0, -H_q)^T$, $g = (H_p, 0)^T$. If H_p is independent of q, then we obtain an explicit scheme which still retains some advantages of the implicit one.

□

We now proceed to construct some instances of our IMEX RK family of schemes. We will use the triplet (s, σ, p) to identify a scheme (2.1), where s is the number of stages of the implicit scheme, σ is the number of explicit scheme stages (so $\sigma = s+1$ for Case 1, i.e. (2.2), and $\sigma = s$ for Case 2, i.e. (2.3)-(2.4) above), and p is the combined order of the scheme.

2.1 Forward-Backward Euler (1,1,1)

The pair of backward and forward Euler schemes

$$\begin{array}{c|c} 1 & 1 \\ \hline & 1 \end{array} \qquad \qquad \begin{array}{c|c} 0 & 0 \\ \hline & 1 \end{array}$$

can be padded to read

$$\begin{array}{c|cc} 0 & 0 & 0 \\ 1 & 0 & 1 \\ \hline & 0 & 1 \end{array} \qquad \qquad \begin{array}{c|cc} 0 & 0 & 0 \\ 1 & 1 & 0 \\ \hline & 1 & 0 \end{array}$$

This yields the linear one-step IMEX (cf. [2]):

$$u_n = u_{n-1} + k(f(u_{n-1}) + g(u_n)).$$

Note that this scheme satisfies (2.3).

2.2 Forward-Backward Euler (1,2,1)

The above form of Euler's method does not satisfy $\hat{b} = \tilde{b}$. The variant that does is

$$\begin{array}{c|cc} 0 & 0 & 0 \\ 1 & 0 & 1 \\ \hline & 0 & 1 \end{array} \qquad \qquad \begin{array}{c|cc} 0 & 0 & 0 \\ 1 & 1 & 0 \\ \hline & 0 & 1 \end{array}$$

i.e. $u_n = u_{n-1} + k(g(u_1) + f(u_1))$ where $u_1 = u_{n-1} + kg(u_1) + kf(u_{n-1})$. This scheme involves an additional evaluation of f per step, compared to the previous one.

2.3 Implicit-Explicit Midpoint (1,2,2)

The Euler pairs are first-order accurate and the (1,1,1) scheme has well-known disadvantages when $g = 0$ (cf. §3 and [2]). The following pair of implicit-explicit schemes

$$\begin{array}{c|cc} 0 & 0 & 0 \\ \frac{1}{2} & 0 & \frac{1}{2} \\ \hline & 0 & 1 \end{array} \qquad \begin{array}{c|cc} 0 & 0 & 0 \\ \frac{1}{2} & \frac{1}{2} & 0 \\ \hline & 0 & 1 \end{array}$$

correspond to applying explicit midpoint for f and implicit midpoint for g. It is second-order accurate because the two schemes from which it is composed are each second-order accurate and $\hat{c} = \tilde{c}$ [7]. This scheme performs usually comparably to the unreasonably popular CNAB considered in [2], and has better symmetry properties.

Example 2.2 *Applying the scheme (1,2,2) to the separable Hamiltonian system*

$$\dot{q} = H_p(p), \quad \dot{p} = -H_q(q)$$

and defining

$$u = \begin{pmatrix} q \\ p \end{pmatrix}, \; f = \begin{pmatrix} H_p \\ 0 \end{pmatrix}, \; g = \begin{pmatrix} 0 \\ -H_q \end{pmatrix},$$

we obtain

$$\hat{K}_1 = \begin{pmatrix} H_p(p_{n-1}) \\ 0 \end{pmatrix}, \quad K_1 = \begin{pmatrix} 0 \\ -H_q(q_1) \end{pmatrix},$$

$$\begin{pmatrix} q_1 \\ p_1 \end{pmatrix} = \begin{pmatrix} q_{n-1} \\ p_{n-1} \end{pmatrix} + \frac{k}{2}(K_1 + \hat{K}_1) = \begin{pmatrix} q_{n-1} \\ p_{n-1} \end{pmatrix} + \frac{k}{2} \begin{pmatrix} H_p(p_{n-1}) \\ -H_q(q_1) \end{pmatrix}$$

$$\hat{K}_2 = \begin{pmatrix} H_p(p_1) \\ 0 \end{pmatrix}, \; \begin{pmatrix} q_n \\ p_n \end{pmatrix} = \begin{pmatrix} q_{n-1} \\ p_{n-1} \end{pmatrix} + k(K_1 + \hat{K}_2) = \begin{pmatrix} q_{n-1} \\ p_{n-1} \end{pmatrix} + k \begin{pmatrix} H_p(p_1) \\ -H_q(q_1) \end{pmatrix}.$$

We note that this scheme is explicit, and it can also be shown to be symplectic. It is identical to the leapfrog/Verlet scheme [12]

$$\begin{aligned} p_n &= p_{n-1} - kH_q(q_{n-1} + k/2H_p(p_{n-1})) \\ q_n &= q_{n-1} + kH_p\left(\frac{p_n + p_{n-1}}{2}\right). \end{aligned}$$

□

2.4 A third-order combination (2,3,3)

The two-stage, third-order DIRK scheme with the best damping properties turns out to be the DIRK scheme (p. 207, [7])

$$\begin{array}{c|cc} \gamma & \gamma & 0 \\ 1-\gamma & 1-2\gamma & \gamma \\ \hline & 1/2 & 1/2 \end{array}$$

with $\gamma = \frac{3+\sqrt{3}}{6}$. For the test equation $\dot{u} = \alpha u$, if we let $z = \alpha k$, then as $z \to -\infty$, $R(\infty) = 1 - \sqrt{3} \approx -0.7321$. This is a marked improvement over the midpoint scheme (1,2,2) which has no attenuation at the stiffness limit ∞.

The corresponding third-order explicit Runge-Kutta scheme (ERK) is

$$\begin{array}{c|ccc} 0 & 0 & 0 & 0 \\ \gamma & \gamma & 0 & 0 \\ 1-\gamma & \gamma-1 & 2(1-\gamma) & 0 \\ \hline & 0 & 1/2 & 1/2 \end{array}$$

The resulting IMEX combination is third-order accurate, has some dissipation near the imaginary axis (like all three-stage third-order ERK methods) and has some attenuation of the stability function at ∞.

2.5 L-stable, two-stage, second-order DIRK (2,3,2)

One may be concerned that the attenuation that the above scheme has may not be sufficient for some problems. A two-stage, second-order DIRK scheme which is stiffly accurate is (p. 106 [8])

$$\begin{array}{c|cc} \gamma & \gamma & 0 \\ 1 & 1-\gamma & \gamma \\ \hline & 1-\gamma & \gamma \end{array}$$

where $\gamma = \frac{2-\sqrt{2}}{2}$. The corresponding three-stage second-order ERK is

$$\begin{array}{c|ccc} 0 & 0 & 0 & 0 \\ \gamma & \gamma & 0 & 0 \\ 1 & \delta & 1-\delta & 0 \\ \hline & 0 & 1-\gamma & \gamma \end{array}$$

Varying δ to get a dissipative stability region, we match the terms of the exponential in the stability function up to third order. This yields the stability region of a three-stage, third-order explicit RK scheme, with $\delta = -2\sqrt{2}/3$. The resulting IMEX combination is second-order accurate.

2.6 L-stable, two-stage, second-order DIRK (2,2,2)

We use the same form (with the same γ but with δ not yet specified) as in the previous IMEX scheme, except for requiring that (2.3) hold instead of (2.2), i.e., $\hat{b}_1 = \delta, \hat{b}_2 = 1-\delta, \hat{b}_3 = 0$. This gives a second-order scheme

$$\begin{array}{c|cc} \gamma & \gamma & 0 \\ 1 & 1-\gamma & \gamma \\ \hline & 1-\gamma & \gamma \end{array} \qquad \begin{array}{c|ccc} 0 & 0 & 0 & 0 \\ \gamma & \gamma & 0 & 0 \\ 1 & \delta & 1-\delta & 0 \\ \hline & \delta & 1-\delta & 0 \end{array}$$

with $\delta = 1 - \frac{1}{2\gamma}$.

2.7 L-stable, three-stage, third-order DIRK (3,4,3)

We would now like to exploit the larger dissipativity region, which four-stage, fourth-order ERK schemes have near the imaginary axis . A three-stage, third-order DIRK scheme which is stiffly accurate is (p. 106 [8])

$$\begin{array}{c|ccc} \gamma & \gamma & 0 & 0 \\ \frac{(1+\gamma)}{2} & \frac{(1-\gamma)}{2} & \gamma & 0 \\ 1 & b_1(\gamma) & b_2(\gamma) & \gamma \\ \hline & b_1(\gamma) & b_2(\gamma) & \gamma \end{array}$$

where γ is the middle root of $6x^3 - 18x^2 + 9x - 1 = 0$, $b_1(\gamma) = -\frac{3}{2}\gamma^2 + 4\gamma - \frac{1}{4}$ and $b_2(\gamma) = \frac{3}{2}\gamma^2 - 5\gamma + \frac{5}{4}$. Numerically, this evaluates to

$$\begin{array}{c|ccc} .4358665215 & .4358665215 & 0 & 0 \\ .7179332608 & .2820667392 & .4358665215 & 0 \\ 1 & 1.208496649 & -.644363171 & .4358665215 \\ \hline & 1.208496649 & -.644363171 & .4358665215 \end{array}$$

The corresponding four-stage, third-order ERK, constructed such that it has the same (desirable) stability region as all four-stage, fourth-order ERK schemes, is

$$\begin{array}{c|cccc} 0 & 0 & 0 & 0 & 0 \\ \gamma & \gamma & 0 & 0 & 0 \\ \frac{(1+\gamma)}{2} & \hat{a}_{31}(\gamma) & \hat{a}_{32}(\gamma) & 0 & 0 \\ 1 & \hat{a}_{41}(\gamma) & \hat{a}_{42} & \hat{a}_{43} & 0 \\ \hline & 0 & b_1(\gamma) & b_2(\gamma) & \gamma \end{array}$$

The third-order conditions indicate that this is a two-parameter family of schemes. Taking our degrees of freedom to be $\hat{a}_{42}, \hat{a}_{43}$, the remaining expressions are

$$\hat{a}_{31} = \left(1 - \frac{9}{2}\gamma + \frac{3}{2}\gamma^2\right)\hat{a}_{42} + \left(\frac{11}{4} - \frac{21}{2}\gamma + \frac{15}{4}\gamma^2\right)\hat{a}_{43} - \frac{7}{2} + 13\gamma - \frac{9}{2}\gamma^2,$$

$$\hat{a}_{32} = \left(-1 + \frac{9}{2}\gamma - \frac{3}{2}\gamma^2\right)\hat{a}_{42} + \left(-\frac{11}{4} + \frac{21}{2}\gamma - \frac{15}{4}\gamma^2\right)\hat{a}_{43} + 4 - \frac{25}{2}\gamma + \frac{9}{2}\gamma^2,$$

$$\hat{a}_{41} = 1 - \hat{a}_{42} - \hat{a}_{43}.$$

Selecting particular values for $\hat{a}_{42}(\gamma)$ and $\hat{a}_{43}(\gamma)$ so as to match the terms of the exponential in the stability function up to fourth order, we obtain the scheme

$$\begin{array}{c|cccc}
0 & 0 & 0 & 0 & 0 \\
.4358665215 & .4358665215 & 0 & 0 & 0 \\
.7179332608 & .3212788860 & .3966543747 & 0 & 0 \\
1 & -.105858296 & .5529291479 & .5529291479 & 0 \\
\hline
 & 0 & 1.208496649 & -.644363171 & .4358665215
\end{array}$$

The resulting IMEX combination is third-order accurate.

2.8 A four-stage, third-order combination (4,4,3)

No pair consisting of a three-stage, L-stable DIRK and a four-stage ERK satisfying (2.3) with a combined third-order accuracy could be found. In order to obtain a third-order formula satisfying (2.3), we need to go to a four-stage, third-order, L-stable DIRK, coupled with a four-stage ERK in the manner indicated in Case 2 of §2. After having satisfied the order conditions and imposed L-stability, we are left with a few families of schemes.

Experimenting with the test equation of §3, we have selected a scheme which has rational coefficients which are not too large, and a diagonal entry which is close to that of the four-stage, *fourth-order*, L-stable DIRK. In particular, we have chosen $c_1 = \frac{1}{2}$, accompanied by the choices $c_3 = \frac{1}{2}$, $b_4 = \frac{1}{2}$, and $\hat{a}_{43} = \frac{1}{2}$. The resulting scheme is

$$\begin{array}{c|cccc}
\frac{1}{2} & \frac{1}{2} & 0 & 0 & 0 \\
\frac{2}{3} & \frac{1}{6} & \frac{1}{2} & 0 & 0 \\
\frac{1}{2} & -\frac{1}{2} & \frac{1}{2} & \frac{1}{2} & 0 \\
1 & \frac{3}{2} & -\frac{3}{2} & \frac{1}{2} & \frac{1}{2} \\
\hline
 & \frac{3}{2} & -\frac{3}{2} & \frac{1}{2} & \frac{1}{2}
\end{array}$$

$$\begin{array}{c|ccccc}
0 & 0 & 0 & 0 & 0 & 0 \\
\frac{1}{2} & \frac{1}{2} & 0 & 0 & 0 & 0 \\
\frac{2}{3} & \frac{11}{18} & \frac{1}{18} & 0 & 0 & 0 \\
\frac{1}{2} & \frac{5}{6} & -\frac{5}{6} & \frac{1}{2} & 0 & 0 \\
1 & \frac{1}{4} & \frac{7}{4} & \frac{3}{4} & -\frac{7}{4} & 0 \\
\hline
 & \frac{1}{4} & \frac{7}{4} & \frac{3}{4} & -\frac{7}{4} & 0
\end{array}$$

3 Test equation for convection-diffusion

As is shown in [2], using a centered discretization scheme for the spatial derivatives of advection-diffusion PDEs, a von Neumann analysis yields that a simple yet appropriate test equation is the scalar ODE (1.2) with

$$f = \mathrm{i}\beta u, \quad g = \alpha u,$$

where α, β are real constants, usually $\alpha \leq 0$, $\beta > 0$, and $\mathrm{i} = \sqrt{-1}$. [1]

For a given time step k, we can define

$$x = k\alpha, \quad y = k\beta, \quad z = x + \mathrm{i}y,$$

and write an IMEX step (2.1)-(2.2) as

$$u_n = u_{n-1} + z\sum_{j=1}^{s} b_j u_j \equiv R(z)u_{n-1}, \tag{3.1}$$

where

$$u_i = \frac{(1+\mathrm{i}y\hat{a}_{i+1,1})u_{n-1} + \sum_{j=1}^{i-1}(xa_{ij} + \mathrm{i}y\hat{a}_{i+1,j+1})u_j}{1 - xa_{ii}} \qquad i = 1, \ldots, s. \tag{3.2}$$

For schemes where $\sigma = s$, i.e. where (2.3) holds, an expression like (3.1) need not be used because $u_n = u_s$.

Let us consider the two Euler schemes first. For the usual pair (1,1,1), equation (3.2) implies

$$u_n = \frac{1+\mathrm{i}y}{1-x}u_{n-1}.$$

On the imaginary axis, $|u_n| \leq (1+y^2)|u_{n-1}|$, and the scheme is unconditionally unstable for any $y \neq 0$ (cf. [2]). As $x \to -\infty$ and with y bounded, however, the scheme is unconditionally stable and $u_n \to 0$, i.e. attenuation compatible with that of the exact solution is realized. For the other pair, (1,2,1), we get from (3.1)-(3.2)

$$u_n = \left(1 + z\frac{1+\mathrm{i}y}{1-x}\right)u_{n-1}.$$

Setting $x = 0$ initially, we obtain that, along the imaginary axis,

$$|u_n|^2 \leq (1 - y^2 + y^4)|u_{n-1}|^2,$$

[1] W. Hunsdorfer (Workshop on Innovative Time Integrators, CWI, Amsterdam, 1996) has indicated that a more general test equation where α and β are allowed to be complex is useful, but we stay with the simpler test equations and lend further support to the analysis with more general numerical experiments in the following sections.

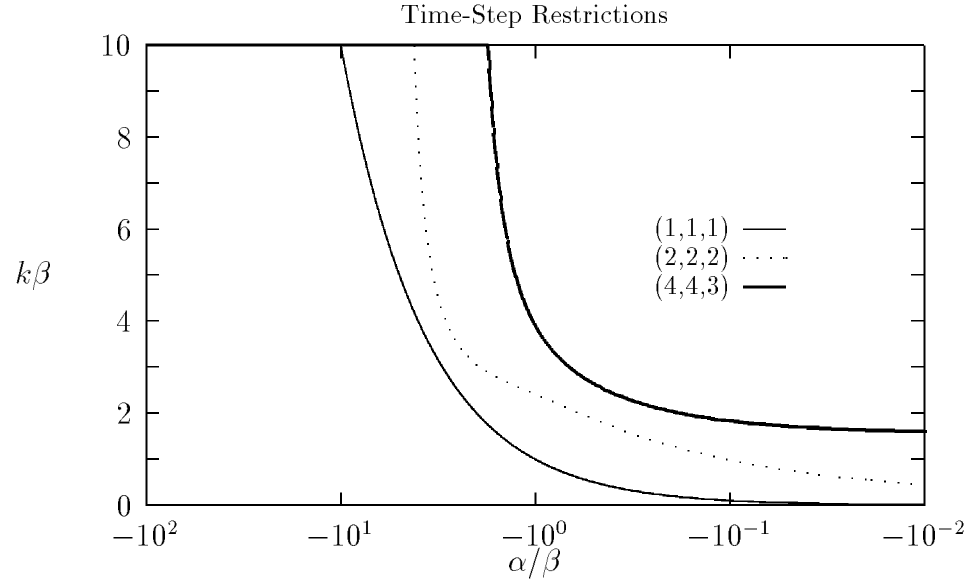

Figure 3.1: Time-step stability restrictions for various values of α and β, for IMEX schemes satisfying (2.3). Note that all these schemes perform well in the high-attenuation limit.

so stability is achieved provided that

$$|y| \leq 1.$$

This corresponds to the CFL condition. On the other hand, letting $x \to -\infty$, we also obtain the restriction $|y| \leq 1$ in the high-attenuation limit. Thus, we see that the variant (1,2,1) has stability characteristics which are preferable over the usual backward-forward Euler scheme in the hyperbolic limit and worse in the parabolic limit.

Now, we can ask, given a fixed ratio $x/y = \alpha/\beta$, what is the maximum $y > 0$ for which the scheme is stable, i.e. $|R(z)| < 1$? This gives the stability restriction on the step-size for a given problem. In Figure 3.1, we plot the resulting curves for the IMEX scheme presented earlier of the second type, i.e. those satisfying (2.3). Corresponding curves for the schemes satisfying (2.2) are plotted in Figure 3.2.

Common to all the schemes in Figure 3.2 is that, as $\alpha \to -\infty$, there is a time-step restriction involving β, typically $k\beta < 1$. In contrast, no such restriction occurs for schemes satisfying (2.3), and hence (2.4), in Figure 3.1. The behavior of these latter schemes is qualitatively similar in the high-attenuation limit to that of the SBDF schemes [2]. On the other hand, the scheme (3,4,3) in Figure 3.2 suggests a potential advantage, in terms of allowable time steps, over a large range of parameter values.

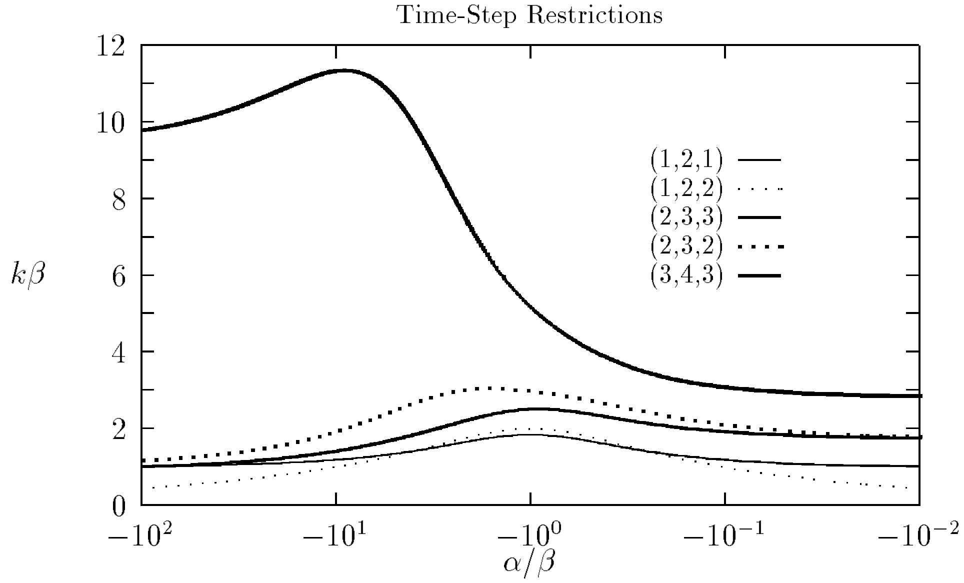

Figure 3.2: Time-step stability restrictions for various values of α and β, for IMEX schemes satisfying (2.2). Note that some of these schemes, especially (3,4,3), perform well when $-\alpha$ is not too large in magnitude, but they all have time-step restrictions in the high-attenuation limit.

4 Finite-Difference Approximations in 1D

4.1 A linear problem

Consider the one-dimensional variable-coefficient problem

$$u_t + \sin(2\pi x)u_x = \nu u_{xx}, \tag{4.1}$$

subject to periodic boundary conditions on the interval [0,1] and initial condition

$$u(x,0) = \sin(2\pi x).$$

We use centered, second-order differences for the spatial derivatives. Note that the solution is smooth for all $\nu \geq 0$.

Large-viscosity examples

To examine the behavior of IMEX RK schemes for large viscosities[2], the model problem (4.1) was approximated using the time step $k = 1.8h_0$, $h_0 = \frac{1}{63}$. For the spatial

[2]By *large viscosity*, we mean that the mesh Reynolds number is small (< 2; see e.g. [2]). An estimate for the mesh Reynolds number is given by $R = \frac{ah}{\nu}$ where ν represents viscosity, a represents characteristic speed, and h represents grid spacing.

discretization, we chose a grid spacing of $h = h_0$, $h_0/2$, $h_0/4$ or $h_0/8$. Utilizing several schemes, computations to time $t = 2$ were performed for viscosities, ν, in the range $.01 \leq \nu \leq .1$. For $h = h_0$, these values correspond to mesh Reynolds numbers, R, in the range $1.59 \geq R \geq 0.159$. For smaller h, R is correspondingly smaller.

The relative errors measured in the maximum norm are plotted against ν in Figure 4.1. In Figure 4.1(a), the errors for the three- and four-stage schemes are omitted since they are always within a factor of 2 of the two-stage, second-order scheme (2,3,2). As expected from the theory of the previous section, the three-stage DIRK (3,4,3) and the schemes satisfying property (2.3) allow for the largest stable time steps when ν is large.

When we decrease h, keeping k fixed, the methods (1,2,2), (2,3,3) and (2,3,2) become unstable over the entire depicted range of ν. Among the stable methods, the higher order of (3,4,3) and (4,4,3) becomes more apparent as the spatial error ceases to dominate the temporal error. For $h = h_0/8$, only the methods satisfying (2.3) remain stable. No effective error reduction is detected for these values of h and k.

Doubling the time step while keeping $h = h_0$ also causes the two-stage methods (2,3,2) and (2,3,3) to become unstable for almost the entire ν-interval depicted. Nonetheless, the three- and four-stage methods remain stable over the entire interval and the scheme (2,2,2) is stable over most of the interval. Even upon tripling the time step (see Figure 4.2), the three- and four-stage schemes are appropriate for approximating strongly-damped flows. Indeed, a comparison with the results of [2] indicates that the three-stage method (3,4,3) is more accurate and stable in this example than the popular CNAB scheme with one-third the step size, even for this relatively coarse step size k.

Small-viscosity examples

To examine the behavior of IMEX RK methods for large mesh Reynolds numbers, example (4.1) was approximated using discretization step sizes $h = \frac{1}{81}$ in space and $k = 1.8h$ in time. Using several IMEX schemes, computations to time $t = 2$ are performed for viscosities, ν, in the range $.001 \leq \nu \leq .01$. These values correspond to mesh Reynolds numbers, R, in the range $12.3 \geq R \geq 1.23$.

The relative errors in maximum norm for these computations are plotted against ν in Figure 4.3. Here, we find that the errors for the third-order schemes and the two-stage, second-order DIRK (2,3,2) nearly coincide since they arise predominantly from the spatial discretization. It is especially noteworthy that the errors for these four schemes are always smaller than those arising for the two-step IMEX schemes considered in [2] even though twice the time step is applied.

4.2 Burgers Equation

Qualitatively similar results to those obtained above for the linear problem (4.1) are obtained for the Burgers equation

$$u_t + uu_x = \nu u_{xx}, \tag{4.2}$$

with which we have experimented, subject to homogeneous Dirichlet boundary conditions and the initial conditions

$$u(x,0) = \sin(\pi x), \qquad 0 < x < 1.$$

For small ν, a boundary layer develops near $x = 1$. This necessitates the use of upwinding. Note that upwinding can be viewed as an addition of a discrete $O(h)$ diffusion term (where h is the spatial step-size) to a centered-difference approximation of uu_x.

5 Time-dependent Multigrid in 2D

We consider the two-dimensional convection-diffusion problem,

$$\mathbf{u_t} + (\mathbf{u} \cdot \nabla)\mathbf{u} = \nu \Delta \mathbf{u}, \tag{5.1}$$

where $\mathbf{u} \equiv (u, v)$. We carry out our computations on the square $\Omega \equiv$[0,1]$\times$[0,1] and consider periodic boundary conditions and the initial conditions

$$\begin{aligned} u(x,y,0) &= \sin[2\pi(x+y)] + 0.005\cos[2\pi(64x+63y)] \\ v(x,y,0) &= \sin[2\pi(x+y)] + 0.005\cos[2\pi(64x+63y)]. \end{aligned}$$

For the spatial discretization, we use standard second-order centered differences. Time-stepping is carried out using a variety of IMEX RK schemes (the convection term, $(\mathbf{u} \cdot \nabla)\mathbf{u}$, is handled explicitly and the diffusion term, $\nu\Delta\mathbf{u}$, is handled implicitly). This treatment yields a positive-definite, symmetric, sparse, linear system to be solved at each stage. Such systems are solved efficiently using a multigrid algorithm, the components of which are outlined in [2].

The model problem (5.1) was approximated using a mesh size $h = \frac{1}{128}$ and a residual tolerance of TOL=0.003 at each stage. The time step was selected to be $k = 0.00625$ to achieve stable results. For several IMEX RK schemes, the average number of fine-grid iterations at each time step was computed. The results for V(1,1)-cycles are provided in the table below. In addition to the schemes developed in §2, we include results for Griepentrog's scheme [6, 7], which is not of the form (2.1).

Scheme	*viscosity, ν*				
	0.01	0.02	0.03	0.04	0.05
Forward-backward Euler (1,1,1)	1.94	1.90	1.71	1.29	1.19
Forward-backward Euler (1,2,1)	1.97	1.94	1.48	1.19	1.19
Implicit-explicit midpoint (1,2,2)	2.23	2.87	3.13	3.29	3.68
Third-order combination (2,3,3)	4.32	4.42	3.68	3.71	3.81
Griepentrog's scheme	4.58	5.23	5.39	5.61	5.90
L-stable, 2-stage, 2nd-order DIRK (2,3,2)	3.81	3.35	2.74	2.58	2.61
L-stable, 2-stage, 2nd-order DIRK (2,2,2)	3.90	3.35	2.81	2.58	2.58
L-stable, 3-stage, DIRK (3,4,3)	5.87	5.35	3.81	3.61	3.58
L-stable, 4-stage, 3rd-order scheme (4,4,3)	7.84	7.35	5.16	4.81	4.77

From the table, we see that the strongly-damping L-stable schemes require the fewest fine-grid iterations per stage for large-viscosity problems. Weakly-damping schemes require far more effort to solve the implicit equations accurately, because lingering high-frequency modes necessitate more work on the finest grid. This is especially evident for the implicit-explicit midpoint scheme (1,2,2) since more than three iterations were required per stage when $\nu \geq 0.03$. Griepentrog's scheme also requires extra fine-grid iterations, presumably to damp out the high-frequency components which arise during the initial stage.

References

[1] S. Abarbanel, D. Gottlieb, and M. Carpenter. On the removal of boundary errors caused by Runge-Kutta integration of nonlinear partial differential equations. *SIAM J. Scient. Comput.*, 17:777–782, 1996.

[2] U. Ascher, S. Ruuth, and B. Wetton. Implicit-explicit methods for time-dependent PDE's. *SIAM J. Numer. Anal.*, 32:797–823, 1995.

[3] C. Canuto, M.Y. Hussaini, A. Quarteroni, and T.A. Zang. *Spectral Methods in Fluid Dynamics*. Springer-Verlag, 1987.

[4] M. Carpenter, D. Gottlieb, S. Abarbanel, and W. Don. The theoretical accuracy of Runge-Kutta time discretizations for the initial-boundary value problem: A study of the boundary error. *SIAM J. Scient. Comput.*, 16:1241–1252, 1995.

[5] M. Crouzeix. Une méthode multipas implicite-explicite pour l'approximation des équations d'évolution paraboliques. *Numer. Math.*, 35:257–276, 1980.

[6] E. Griepentrog. Gemischte Runge-Kutta-verfahren für steife systeme. In *Seminarbereicht Sekt. Math.*, number 11, pages 19–29, Humboldt-Universität Berlin, 1978.

[7] E. Hairer, S.P. Norsett, and G. Wanner. *Solving Ordinary Differential Equations I: Nonstiff Problems.* Springer-Verlag, 1993.

[8] E. Hairer and G. Wanner. *Solving Ordinary Differential Equations II: Stiff and Differential-Algebraic Problems.* Springer-Verlag, 1991.

[9] G.E. Karniadakis, M. Israeli, and S.A. Orszag. High-order splitting methods for the incompressible Navier-Stokes equations. *J. Computational Phys.*, 97:414–443, 1991.

[10] J. Kim and P. Moin. Application of a fractional-step method to incompressible Navier-Stokes equations. *J. Computational Phys.*, 59:308–323, 1985.

[11] S. Ruuth. Implicit-explicit methods for reaction-diffusion problems in pattern formation. *J. Math. Biology*, 34(2):148–176, 1995.

[12] Robert D. Skeel, Guihua Zhang, and Tamar Schlick. A family of symplectic integrators: stability, accuracy, and molecular dynamics applications. *SIAM J. Sci. Comput.*, 18(1):203–222, 1997.

[13] R. Spiteri, U. Ascher, and D. Pai. Numerical solution of differential systems with algebraic inequalities arising in robot programming. In *Proceedings of the IEEE Conference on Robotics and Automation*, 1995.

[14] S. Turek. A comparative study of time stepping techniques for the incompressible Navier-Stokes equations: from fully implicit non-linear schemes to semi-explicit projection methods. *Int. J. Num. Meth in Fluids*, 22:987–1011, 1996.

[15] J.M. Varah. Stability restrictions on second order, three level finite difference schemes for parabolic equations. *SIAM J. Numerical Analysis*, 17(2):300–309, 1980.

[16] J.G. Verwer, J.G. Blom, and W. Hundsdorfer. An implicit-explicit approach for atmospheric transport-chemistry problems. *Applied Numerical Mathematics*, 20:191–209, 1996.

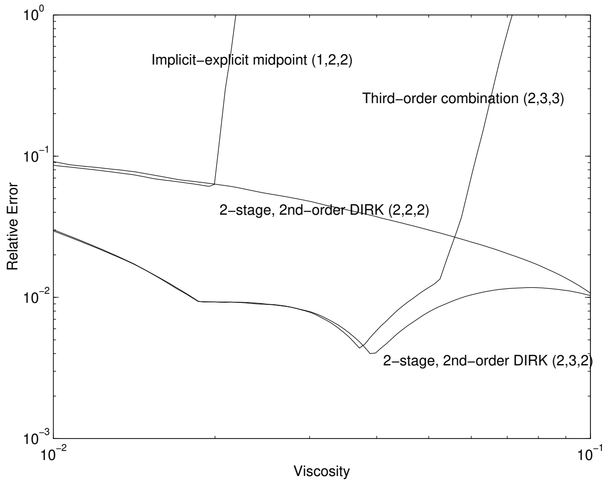

(a) $h = \frac{1}{63}$

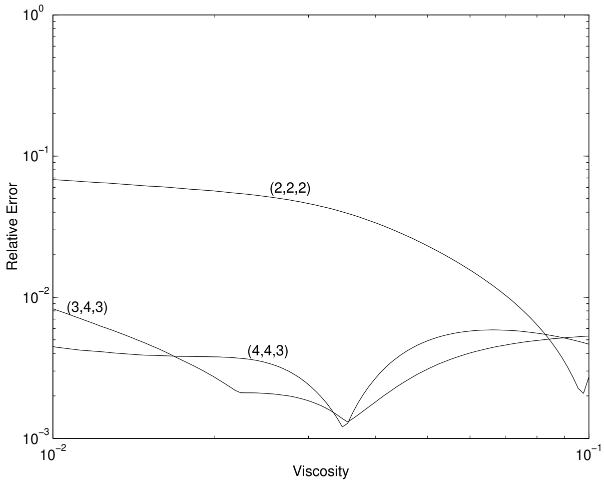

(b) $h = \frac{1}{126}$

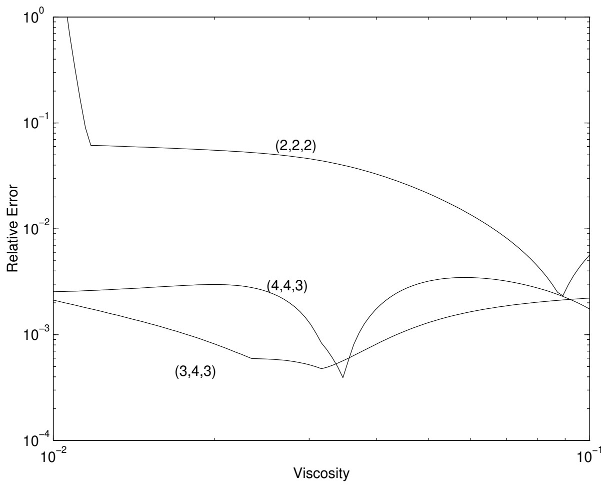

(c) $h = \frac{1}{252}$

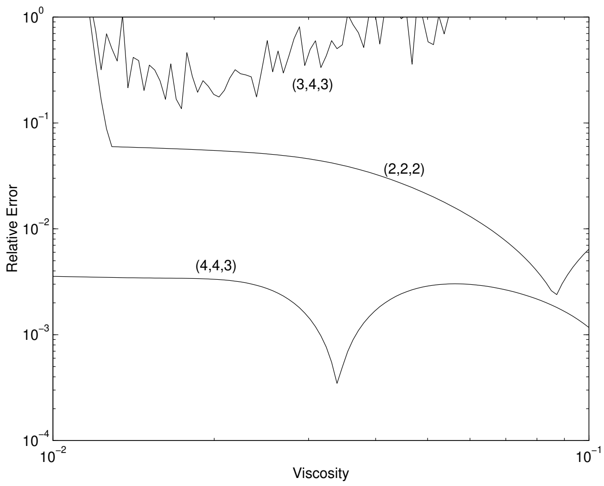

(d) $h = \frac{1}{504}$

Figure 4.1: Large-viscosity behavior for $k = 1.8h_0, h_0 = \frac{1}{63}$

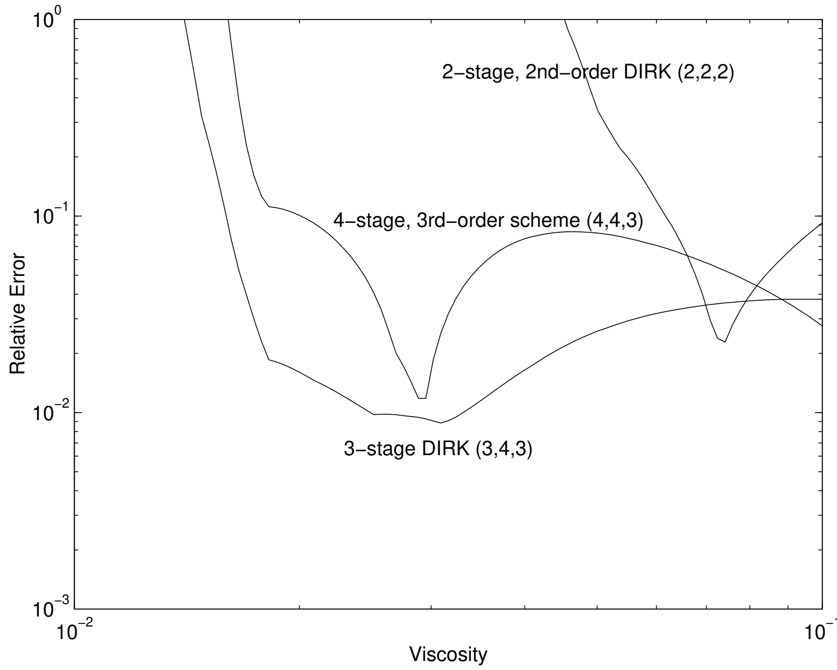

Figure 4.2: Large-viscosity behavior for $k = 5.4h, h = h_0$

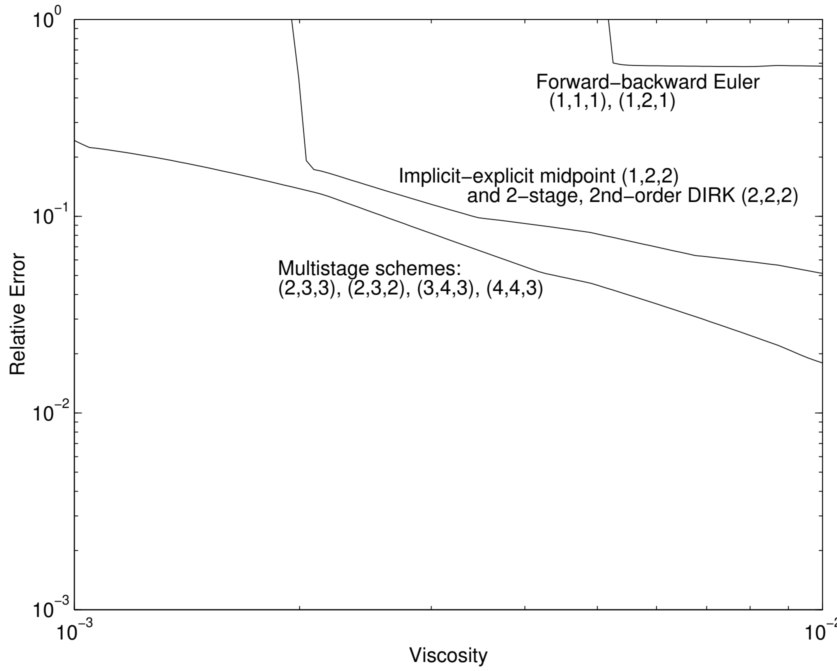

Figure 4.3: Small-viscosity example for $k = 1.8h, h = \frac{1}{81}$